Proceedings of The National Conference
On Undergraduate Research (NCUR) 2016
University of North Carolina Asheville
Asheville, North Carolina
April 7-9, 2016

Constraints On The Quaternary Fault Offset History Along The Benton Springs Right-Lateral Strike-Slip Fault, West-Central Nevada

Timothy J. Daniel
Department of Environmental Studies
University of North Carolina at Asheville
One University Heights
Asheville, North Carolina, 28804 USA

Faculty Advisor: Dr. Jackie Langille

Abstract

The Walker Lane is a ~700 km zone of strike-slip and normal faults that extend southward from northeastern California, through western Nevada, and into eastern California. The Walker Lane is important geologically because it accommodates ~25% of the total movement between the Pacific and North American tectonic plates, the rest being accommodated mostly by the San Andreas fault. While the Walker Lane has been the focus of much research, the evolution of this zone is still unclear and has significant implications for the tectonic evolution of this plate boundary system. Some of this uncertainty comes from the lack of constraints as to the amount and rate of fault displacement, specifically in the central Walker Lane, Nevada. This study utilized field mapping of fault scarps and offset alluvial features combined with detailed surveys of these offset features using Terrestrial Laser Scanning (TLS) to document the magnitude of Quaternary fault offset along a section of the Benton Springs right-lateral strike-slip fault within the central Walker Lane. TLS derived digital elevation models (DEMs) were used to generate hillshade and slope maps which were used to precisely measure the magnitude of the offset by back-slipping and reconstructing offset streams using the published MATLAB GUI, LaDiCaoz. Our results indicate that this portion of the fault records right lateral fault offset magnitudes of ~35, 33, 22, 10, 7, 3, and 1 m. The ~1 m offset likely resulted from the most recent earthquake, while the others accumulated from multiple earthquakes. The offset amount from the last earthquake, combined with offset amounts from other studies along this fault were used to estimate the Richter magnitude of the last earthquake, which equates to a magnitude in the range of 6.1 and 7.1.

Keywords: Walker Lane, Terrestrial Laser Scanning, strike-slip fault offset measurement

1. Introduction

1.1 The San Andreas fault system and the Walker Lane

The San Andreas fault system, which runs through western California to northern Mexico, spans a distance of roughly 800 miles. This fault system accommodates the majority of the ~50 mm/yr of right-lateral motion between the Pacific and North American tectonic plates[1]. In the 1906 San Francisco earthquake, almost 6.4 m of slip was recorded at the Tomales bay road head or the equivalent of about 110 years of movement on this fault, indicating that the release of slip on the fault is episodic and poses significant seismic risk[2]. While the San Andreas accommodates much of the total slip between the Pacific and North American tectonic plates, ~25% of this movement is not accommodated by the San Andreas fault system. Instead, it is accommodated along the faults within the Eastern California shear zone (ECSZ) and Walker Lane[3, 4, 5, 6]. The Walker Lane itself is bordered to the south by the ECSZ, which accommodates fault-slip across several major strike-slip faults and transfers fault slip north into the Walker Lane[7] (Fig. 1). In this paper, the separation between the ECSZ and Walker Lane to the north occurs at the Garlock Fault (Fig. 1).

Observations have concluded that the Walker Lane Block has accrued between 48-60 km of dextral slip within the past 10-15 million years[8]. This paper focuses on the central Walker Lane section which consists of five main right-lateral strike-slip faults, focusing specifically on the Benton Springs fault (Fig. 1).

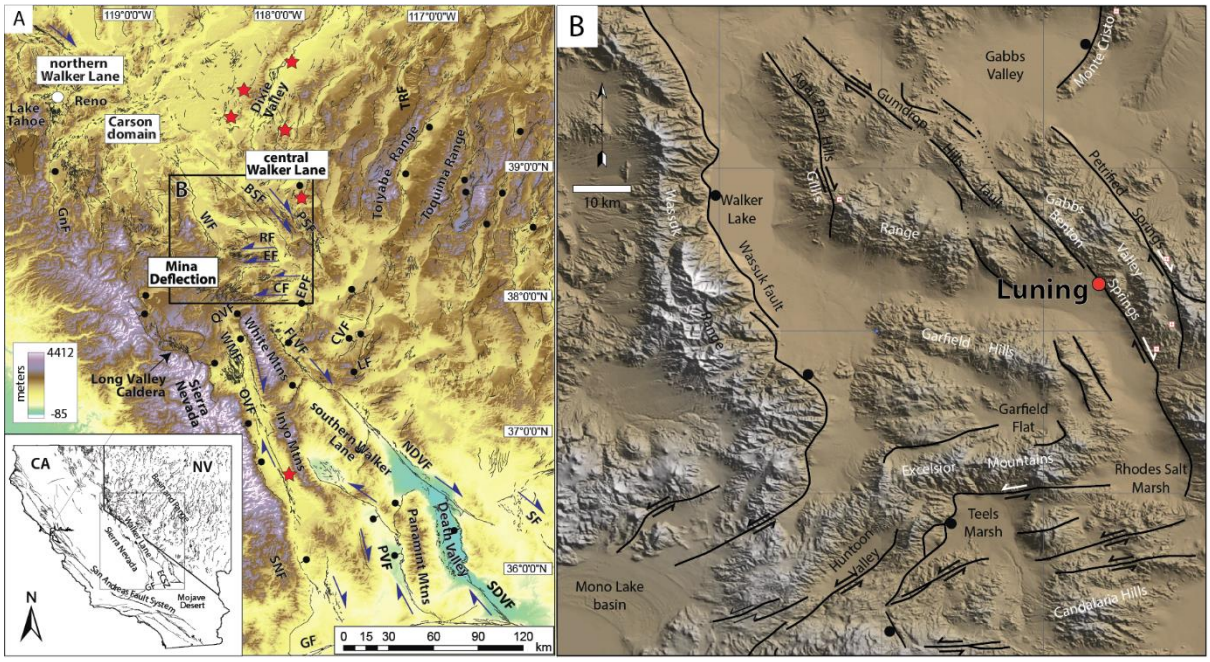

Figure 1. Relief maps showing active faults in the Walker Lane and the Eastern California shear zone (ECSZ). BSF, Benton Springs fault; PSF, Petrified Springs fault; WF, Wassuk fault; GF, Garlock fault. Boxes indicate the location of figures (A) and (B).

Each star in Figure 1A represents a historical >6.0 magnitude earthquake. Arrows indicate strike-side fault movement direction (side-to-side) and balls indicate normal fault motion (extension). Figure 1B shows the location of the Benton Springs fault within the central Walker Lane. The red dot labelled Fig. 2 shows the location of the Luning site in this study.

1.2 The Benton Springs fault

The Benton Springs fault is located adjacent to the Petrified Springs and Gumdrop Hills faults (Fig. 1B). Previous studies estimate that the Benton Springs fault accommodates on average ~1 mm of right-lateral strike-slip movement per year, although it is to be noted that this number is most likely an underestimate due to a lack of age constraints[8]. The fault itself has offset several erosional ridgelines and created several beheaded streams within alluvial deposits shed from the mountains. The faults in this portion of the Walker Lane are not creeping (creeping indicates that there are many small earthquakes) but rather they release built up energy through episodic earthquakes, and often result in complicated surface rupture patterns[9]. A prime example is the 7.2 magnitude earthquake known as the Cedar Mountain earthquake that occurred immediately east of the Benton and Petrified Springs faults in 1932[8,9] (noted by the star within the box B subset of Fig. 1A). The Cedar Mountain earthquake produced a sporadic set of surface ruptures, fissures, and fractures on multiple faults over a 10x70 km area in three different valleys.

1.3 Objectives

This study employed field mapping and high-detailed Terrestrial Laser Scanning (TLS) surveys to generate high-detailed maps of a portion of the Benton Springs fault, from which the magnitudes of fault offset were estimated by reconstructing offset surface features, such as streams and alluvial sedimentary deposits. These data are used here to: (1) constrain the past earthquake history on a section of this fault and (2) to estimate the likely magnitude of the last earthquake. The offset values estimated from this study will be combined in the future with ages of offset features to

constrain the average slip rate on this fault through time, indicating whether or not this fault is speeding up, slowing down, etc. This will have significant implications for the formation of this part of the plate boundary system which may result in further in depth studies in this region.

2. Methods

2.1 Field Mapping and Terrestrial Laser Scanning

Mapping of alluvial surfaces and fault traces was completed both in the field and using digital orthophotographs. Mapping was conducted at the 1:2,000 to 1:5,000 scale. Wesnousky[8] provided a comprehensive overview of the localities along the Benton Springs fault where there are offset alluvial markers. This study builds on his work by conducting detailed mapping and TLS surveying at these localities to provide high-resolution maps to measure right-lateral offset in detail (see Figs. 2, 3, and 4 in results section).

Detailed surveying of the Luning site along the BSF was included in this study (see Fig. 1B for location). TLS is a method in which the geometry of the topography is measured in detail by recording the three-dimensional position of points that lie on the landscape, which make up a laser-derived point cloud. The point cloud is then used for interpolation and generation of high-resolution digital elevation models (DEMs). Point clouds were obtained using a Riegl VZ400 terrestrial laser scanner, which sends and records the return of long-range near infrared laser waveforms from the surface. This instrument yields an accuracy of 5 mm and precision of 3 mm at distances up to 600 m for natural targets with confidence of 1-sigma at 100 m under manufacturer test conditions.

The point clouds recorded were processed using RiSCAN PRO software. Adjacent points closer than 1 cm were merged and cells containing only one point removed. Composite point clouds for each site were generated using multiple scan positions linked by reflector targets along the lengths of interest. These data were then referenced geospatially via GNSS L1/L2 recordings taken at each individual scan location and at three reflector target positions. These GNSS data were then corrected by the OPUS CORS network resulting in uncertainties ranging from 0.5-1 cm. Filters to reduce vegetation and boulders in the point cloud were applied to remove these from the final DEM.

2.2 Offset Measurements

Offsets measurements were made from offset ephemeral stream channels. Offset measurements were performed by back-slipping the DEMs to reconstruct the offset streams, using the methodology and tools presented in Zielke and Arrowsmith[10] and Zielke et al.[11]. Offset reliability was assessed through field observations and the topographic fit of the reconstructions. Offsets were identified from high-resolution aerial imagery and mapped in detail in the field. Slope, hillshade, and contour maps derived from the TLS derived DEMs were used to further detail the fault and offset features. These maps were generated using ESRI ArcGIS software and LiDARImager[10] (e.g. Figs 2 and 3). Back-slipping and offset measurements were made utilizing the MATLAB GUI LaDiCaoz[10]. This GUI calculates an optimal offset based on the goodness of fit (GoF) for back-slipped profiles across offset stream channels (Fig. 3). Back-slipping and visual inspection of offset features was used to define the offset range.

2.3 Earthquake Magnitude Calculations

The amount of offset along a rupture from one earthquake event can vary along the rupture length but the average rupture amount can be used to estimate earthquake magnitude[12,13] using the equation below:

$$M = 6.94 + 1.14 * \log(d_{avg}) \quad (1)$$

where M is the earthquake Richter magnitude and d_{avg} is the average amount of displacement along the rupture from the earthquake event. Equation 1 was extrapolated from the forward and inverse relationships derived from Wells and Coppersmiths[13] equation for magnitude based on the length of the rupture using the equation below:

$$M = 5.08 + 1.16 * \log(L) \quad (2)$$

where M is the earthquake Richter magnitude and L is the length of the surface rupture. Equation 1 was derived from measurements from 77 mapped surface ruptures and equation 2 from 56 mapped ruptures, all from magnitudes ranging from 5.6 to 8.1[12].

3. Results

3.1 Offset Measurements

As explained above, the DEMs were used with the MATLAB GUI LaDiCaoz to calculate the amount of offset of stream channels at the Luning site. LaDiCaoz matches the topographic profile of an offset stream upstream of the fault with that downstream of the fault (Figs. 2 and 3). Based on the goodness of fit (GoF), it produces an optimal offset amount[10, 11]. The minimum and maximum offset amounts were constrained by visual inspection of the potential range of offsets by matching either side of the stream channels.

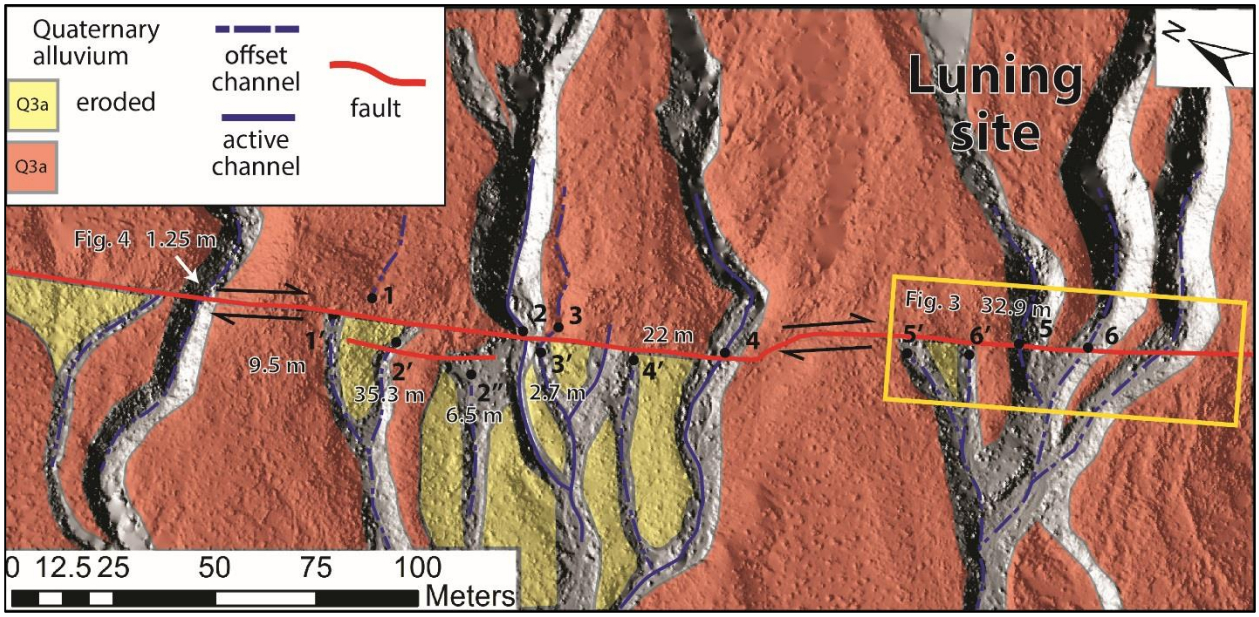

Figure 2. Hillshade map of a portion of the Luning site derived from TLS, showing mapped Quaternary alluvial deposits and offset streams.

The numbers (e.g., 1-1') in Figure 2 denote offset streams that correlate across the fault. The optimal offset amount calculated using LaDiCaoz is included next to the offset marker. Back-slipping and reconstruction of the channels resulted in optimal offset amounts of 1.25, 2.7, 6.5, 9.5, 22, 32.9, and 35.3 m (Figs. 2 and 3, Table 1).

Table 1. Results of LaDiCaoz offset measurement including the optimal, minimum, and maximum offset amounts for offset streams shown in Figure 2

Label	Optimal offset	Maximum offset	Minimum offset
Fig. 4	1.25	1.5	1
1-1’	9.5	11	9
2-2’	35.3	35.6	35
2-2”	6.5	7.7	6.1
3-3’	2.7	3.2	2.2
4-4’	22	23	21
5-5’ and 6-6’	32.9	33.37	32.2

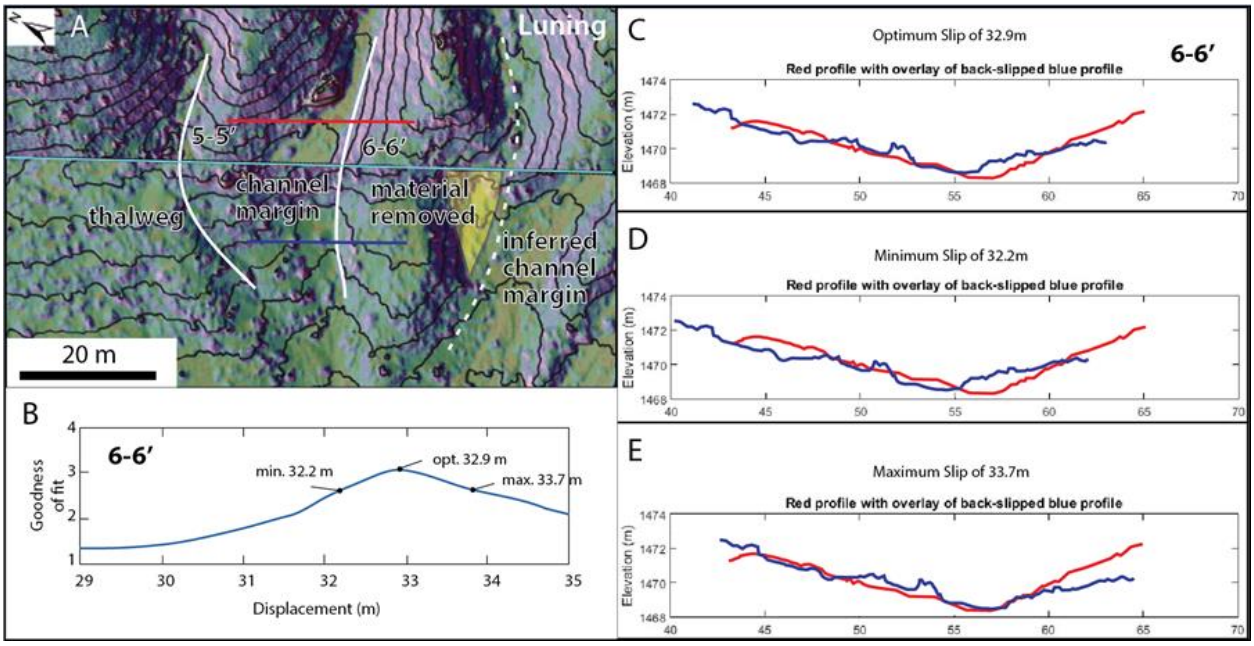

Figure 3. Example of reconstruction and optimal, minimum, and maximum offset measurement using the goodness of fit. Red and blue lines indicate the location of the topographic profiles shown in C through E.

Figure 3A shows the DEM back-slipped by the optimal measurement of 32.9 m. The colors indicate slope or steepness (blues are steep and greens are less steep) and shadowing is the hillshade map. The white lines (Fig. 3A) define the reconstructed thalwegs (lowest part of the channel) for 5-5’ and channel margin for 6-6’. Minimum and maximum were estimated by lining up both sides of the channels.

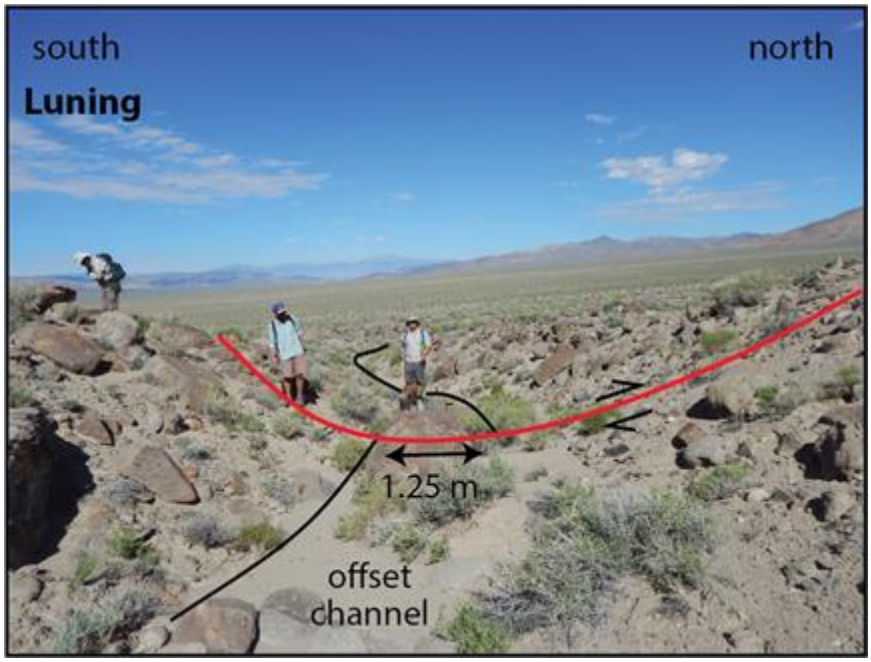

Figure 4. Field photograph showing the 1.25 m offset of a stream channel margin (bold black line) at the Luning site. This offset is interpreted as recording the most recent earthquake event along this section of the fault.

3.2 Magnitude Calculations

Most likely the 1.25 m offset is the result of the most recent earthquake event, while the larger estimates can be seen as culminations of multiple earthquake events. This offset amount appears to be the largest recorded along this fault from the last rupture (Wesnousky[8] documents ~0.2-1 m), assuming these are all from the same rupture event. Equation 1 above was used to calculate the likely Richter magnitude of this earthquake. Because this study only constrained the offset amount at one locality along the rupture from the last earthquake, it does not adequately represent d_{avg}. Instead, this study estimates a range of likely magnitudes from the last earthquake by calculating the magnitude of the earthquake using the offset amount constrained in this study (a maximum of 1.5) along with the minimum offset amount (0.2 m) from other locations along the rupture from other studies[8]. Using 1.5 m and 0.2 m in equation 1 results in a magnitude range of 6.1 to 7.1, similar to that recorded for the 1932 Cedar Mountain earthquake.

4. Discussion

This study suggests that the most recent earthquake resulted in 1.25 m of offset at the Luning site on the Benton Springs fault, which along with other studies[8] equates to a magnitude between 6.1 and 7.1. This is a relatively sizeable quake that fits into the expected and observed range for earthquakes in the central Walker Lane. An earthquake of this size could do some serious damage in an area where there is much more significant infrastructure development and a larger population but luckily much of the Benton Springs fault is sparsely occupied and anticipated damage from shaking is relatively low, excluding a large military ammunitions armory nearby in Hawthorne, NV ~20 miles from the Benton Springs fault.

All of these offsets interpreted from the most recent rupture event occur along a length of ~20 km (found between Dunlap Canyon and Highway 361 from Wesnousky[8]). For comparison, equation 2 above was used to compare the magnitudes calculated above to those calculated based on the approximated rupture length. The estimated earthquake magnitude based on rupture length would be 6.6 which indicates an earthquake magnitude within the range calculated using the offset amount of 0.2-1.25 m, supporting the range of magnitude values calculated here.

Modern earthquake Richter magnitude calculations are based on the amplitude recorded on a seismograph during shaking, which is unknown for earthquakes that occurred prior to modern technology. To test the reliability of using

equations 1 and 2 for earthquake magnitude, rupture length and displacement from the recent magnitude 7.8 earthquake in Kathmandu was used. Because this earthquake occurred recently, the rupture length and displacement were measured using modern seismic techniques. This earthquake had a rupture length of ~160 km[14], estimated from teleseismic P waves. Equation 2 equates to a magnitude of 7.6. Initial models of displacement indicate 2-4 m of thrust motion (one side of the fault is pushed up) along this length[15]. This displacement range equates to magnitudes of 7.2 to 7.6 using equation 1. These estimates are close to the 7.8 magnitude measured from seismic technologies.

The next largest displacement estimate from this study, after the 1.25 m measurement is 2.7 m at 3-3' (Fig. 2). This 2.7 m is the accumulation of at least two earthquakes. If two earthquakes are assumed, the displacement from the first earthquake recorded by this offset would be 1.45 m (2.7 m minus 1.25 m). This would indicate another earthquake within the same magnitude range of the most recent one recorded. Each earthquake along this fault likely had a different amount of displacement, so the total number of earthquake ruptures that accumulated the maximum displacement presented here (35.9 m at 2-2' Fig. 2) cannot be constrained with the present data. However, to have the seven different offset amounts recorded here (Table 1), a minimum of seven earthquake cycles would have occurred since the alluvial fan in which these streams cut was deposited. This is a large underestimate because alluvial features can be eroded away so many of the larger offset values are not preserved.

Age dating of volcanic tephra and charcoal within material shed off of a fault scarp south of the Luning site on the Benton Springs fault by Wesnousky[8] indicates that the most recent rupture happened within the past ~1,000 years.

5. Conclusions

Offset measurements from the Luning site on the Benton Springs fault indicate offset amounts of 1.25, 2.7, 6.5, 9.5, 22, 32.9, and 35.3 m. The smallest amount combined with amounts from Wesnousky[8] (0.2-1.25 m) suggests that this fault is capable of >6.0 magnitude earthquakes. Ongoing work indicates that the other faults in the central Walker Lane, i.e. namely the Petrified Springs, Indian Head, and Gumdrop Hills faults also record offset Quaternary features and are also likely to produce sizeable earthquakes.

By implementing the use of TLS, this study has created some of the first high resolutions DEM's in the central Walker Lane. The data presented here will be combined with future age dating results to help determine the average slip rate on this fault. Age dating will be accomplished via U-series dating of pedogenic carbonate and cosmogenic nuclide age dating of alluvial fan deposits offset by the fault. These results along with offset and rate measurements from the other faults in this portion of the Walker Lane will yield insights into the spatial and temporal evolution of this evolving plate boundary system.

6. Acknowledgements

This study was funded by NSF grant EAR-1419809 awarded to J. Langille and EAR-1419808 awarded to J. Lee. Support was also provided by the University of North Carolina at Asheville. I would like to thank Rex Flake at Central Washington University for providing assistance with TLS data collection and processing, Thomas O'Shea for assistance in field mapping, Jeff Lee of Central Washington University for assistance in field mapping, Kim Blisniuk along with the students of San Jose State University for their assistance in field mapping, and Dr. Jackie Langille for the opportunity to conduct this research.

7. References

1. DeMets, C., and Dixon, T., 1999, New kinematic models for Pacific-North America motion from 3 Ma to present, I: Evidence for steady motion in biases in the NUVEL-1A model: Geophysical Research Letters, v. 26, p. 1921-1924.

2. Schulz, S., Wallace, R., updated 2013, The San Andreas Fault: U.S. Geological Survey: http://pubs.usgs.gov/gip/earthq3/safaultgip.html.

3. Oldow, J., Aiken, C., Hare, J., Ferguson, J., and Hardyman, R., 2000, Active Displacement Transfer and Differential Block Motion Within the Central Walker Lane, Western Great Basin: Geology, v. 22, p. 637-640.

4. Bennet, R., Wernicke, B., and Davis, J., 1998, Continuous GPS measurements of contemporary deformation across the northern Basin and Range province: Geophysical Research Letters, v. 25, p. 563-566.
5. Bennet, R., Wernicke, B., Niemi, N., Frederich, M., and Davis, J., 2003, Contemporary strain rates in the northern Basin and Range province from GPS data: Tectonics, v. 22, doi: 10.1029/2001TC001355.
6. Dixon, T., Robaudo, S., Lee, J., and Reheis, M., 1995, Constraints on present-day Basin and Range deformation from space geodesy: Tectonics, v. 14, p. 755-772.
7. Wesnousky, S., 2005, The San Andreas and Walker Lane Fault Systems. Western North America: Transpression, Transtension, Cumulative Slip and the Structural Evolution of a Major Transform Plate Boundary: Journal of Structural Geology, v. 27, p. 1505-1512.
8. Wesnousky, S., 2005, Active Faulting in the Walker Lane: Tectonics, v. 24, p. 1-35.
9. Bell, J., DePolo, C., Ramelli, A., Sarna-Wojcicki, A., and Meyer, C., 1999, Surface Faulting and Paleoseismic History of the 1932 Cedar Mountain Earthquake Area, West-Central Nevada, and Implications for Modern Tectonics of the Walker Lane: Geological Society of America Bulletin, v. 111, i. 6, p.791-807.
10. Zielke, O., and Arrowsmith, R., 2012, LaDiCaoz and LiDARimager–MATLAB GUIs for LiDAR data handling and lateral displacement measurement: Geosphere, v. 8, p. 206-221.
11. Zielke, O., Arrowsmith, R., Ludwig, L., and Akciz, S., 2012, High-resolution topography-derived offsets along the 1857 Fort Tejon earthquake rupture trace, San Andreas Fault: Bulletin of the Seismological Society of America, v. 102, p. 1135-1154.
12. Biasi, G., and Weldon, R., 2006, Estimating Surface Rupture Length and Magnitude of Paleoearthquakes from Point Measurement of Rupture Displacement: Bulletin of the Seismological Society of America, v. 96, p. 1612-1623.
13. Wells, D., and Coppersmith, K., 1994, New Empirical Relationships among Magnitude, Rupture Length, Rupture Width, Rupture Area, and Surface Displacement: Bulletin of Seismological Society of America, v. 84, p. 974-1002.
14. Fan, W., and Shearer, P., 2015, Detailed rupture imaging of the 25 April Nepal earthquake using teleseismic P waves: Geophysical Research Letters, v. 42, p. 5744-5752.
15. Lindsey, E., Natsuaki, R., Shimada, M., Hashimoto, M., Melgar, D., and Sandwell, T., 2015, Line-of-sight displacement from ALOS-2 interferometry: M_w 7.8 Gorkha Earthquake and M_w 7.3 aftershock: Geophysical Research Letters, v. 42, p. 6655-6661.